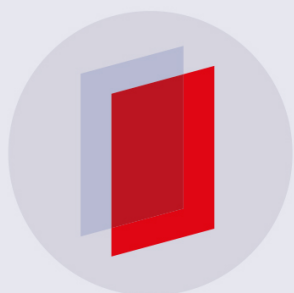


PAPER

# Thin-film growth and structural characterization of a novel layered iridate $\text{Ba}_7\text{Ir}_3\text{O}_{13+\delta}$

To cite this article: Ludi Miao *et al* 2019 *Semicond. Sci. Technol.* **34** 025002

View the [article online](#) for updates and enhancements.



**IOP | ebooks™**

Bringing you innovative digital publishing with leading voices to create your essential collection of books in STEM research.

Start exploring the collection - download the first chapter of every title for free.

# Thin-film growth and structural characterization of a novel layered iridate $\text{Ba}_7\text{Ir}_3\text{O}_{13+\delta}$

Ludi Miao<sup>1</sup> , Yan Xin<sup>2,6</sup>, Jinyu Liu<sup>1</sup>, Huiwen Zhu<sup>1,3</sup>, Hong Xu<sup>1,4</sup>, Diyar Talbayev<sup>1</sup>, Taras Stanislavchuk<sup>5</sup>, Andrei Sirenko<sup>5</sup>, Venkata Puli<sup>1</sup> and Zhiqiang Mao<sup>1,6</sup>

<sup>1</sup>Department of Physics and Engineering Physics, Tulane University, New Orleans, LA 70118, United States of America

<sup>2</sup>National High Magnetic Field Laboratory, Florida State University, Tallahassee, FL 32310, United States of America

<sup>3</sup>Department of Physics, Zhejiang Sci-Tech University, Hangzhou 310018, People's Republic of China

<sup>4</sup>Institute of Laser Engineering, Beijing University of Technology, Beijing 100124, People's Republic of China

<sup>5</sup>Department of Physics, New Jersey Institute of Technology, Newark, NJ 07102, United States of America

E-mail: [zmao@tulane.edu](mailto:zmao@tulane.edu) and [xin@magnet.fsu.edu](mailto:xin@magnet.fsu.edu)

Received 10 July 2018, revised 27 November 2018

Accepted for publication 10 December 2018

Published 7 January 2019



CrossMark

## Abstract

Iridates have attracted immense interest since their strong spin-orbit coupling (SOC) can lead to rich exotic phenomena such as a  $J_{\text{eff}} = 1/2$  Mott insulating state. Here we report a novel iridate discovered in our efforts which aimed to synthesize  $\text{Ba}_2\text{IrO}_4$  thin films. Through systematic transmission and scanning transmission electron microscopy studies, we have shown this new compound possesses a layered orthorhombic structure with the composition of  $\text{Ba}_7\text{Ir}_3\text{O}_{13+\delta}$  (BIO). This material is an insulator with an optical band gap of  $\sim 1.3$  eV. Furthermore, we found that the thin films of this material can be grown on differently orientated perovskite substrates or MgO substrates. Although all these films maintain an identical crystallographic orientation, i.e. its  $c$ -axis perpendicular to the substrate surface, they form various domain structures dependent on the substrate. When (001)-oriented  $\text{LaAlO}_3$  and (111) oriented  $\text{SrTiO}_3$  perovskites are used as substrates, the domains show 12 fold and 6 fold symmetry respectively, and the domain orientations are highly coherent and the domain-walls are atomically sharp. However, the films on the (110) oriented MgO substrates feature much less coherent domain walls and thread dislocations occur at the domain boundaries. These findings not only reveal a new playground for the study of the novel SOC physics of iridates, but also provide a route to tailor the domain wall structure via epitaxial lattice mismatch in films.

Keywords: iridate, thin films, transmission electron microscopy

(Some figures may appear in colour only in the online journal)

## 1. Introduction

Iridates have attracted great attention in recent years due to their novel physics arising from spin-orbital coupling (SOC). In comparison with  $3d/4d$  transition metal oxides (TMOs)

such as cuprates, manganites and ruthenates,  $5d$  electrons in iridates have remarkably enhanced SOC though their electron-electron Coulomb interaction  $U$  slightly decreases [1]. The SOC energy  $\lambda_{\text{SOC}}$  for Ir  $5d$  electrons is  $\sim 0.4$  eV, which is comparable to  $U$  ( $\sim 0.5$  eV) [2, 3]. The interplay between SOC and  $U$  are expected to drive iridates to unique quantum states. A prominent, experimentally established example is

<sup>6</sup> Authors to whom any correspondence should be addressed.

the  $J_{\text{eff}} = 1/2$  Mott insulator induced by SOC in  $\text{Sr}_2\text{IrO}_4$  [2, 4]. Furthermore, exotic phases tuned from SOC-induced Mott states are also predicted, such as topological insulating states [5–8], a topological Weyl semimetal state [9], spin liquid states in the Kitaev limit [10], and unconventional superconductivity [11]. As far as we know, recent experimental studies have suggested hyperhoneycomb  $\beta\text{-Li}_2\text{IrO}_3$  is in close proximity to the Kitaev spin liquid [12]; however, other predicted exotic phenomena have not yet been found in any known iridate systems. Therefore, exploring novel insulating iridate phases may open up a new route to seek novel functional properties of iridates.

In this letter, we report a novel layered iridate  $\text{Ba}_7\text{Ir}_3\text{O}_{13+\delta}$  (BIO), which possesses a layered orthorhombic structure and shows insulating behavior with a band gap of  $\sim 1.3$  eV. In addition, we find that thin films of this material can be grown on both differently-oriented perovskite or MgO substrates. Although the crystallographic orientations of these films remain identical, i.e. its  $c$ -axis perpendicular to the substrate surface, the films form distinct domain structures on different substrates. The films on (111)-oriented  $\text{SrTiO}_3$  (STO) and (001)-oriented  $\text{LaAlO}_3$  (LAO) substrates exhibits highly coherent domains with 6 fold and 12 fold symmetries respectively and the domain-walls are atomically thin. However, the films on the (110)-oriented MgO show much less coherent domains and thread dislocations are observed at the domain-walls. These results not only unveil a new platform for investigating novel SOC physics in iridates, but also suggest a promising route to engineer domain-walls using epitaxial lattice mismatch.

## 2. Experimental

We have grown BIO/STO (111), BIO/LAO (001) and BIO/MgO (110) films using the pulsed laser deposition (PLD) method with a KrF excimer laser ( $\lambda = 248$  nm). A ceramic pellet with the nominal composition of  $\text{Ba}_2\text{IrO}_4$  was used as a PLD target. The films were deposited at  $1080^\circ\text{C}$  in the atmosphere of 150 mTorr of  $\text{O}_2$ . The laser pulse has an energy density of  $0.7\text{ J cm}^{-2}$ , with a repetition rate of 10 Hz. All the films we synthesized are around 277 nm thick. The crystal phase and microstructures of the films are investigated by transmission and scanning transmission electron microscopy (TEM/STEM), and high resolution x-ray diffraction (HR-XRD). Chemical compositions were determined by field-emission SEM. The crystal phase is the same for all three types of films on different substrates. The optical conductivity of the films was measured using a variable-incidence-angle ellipsometry at room temperature.

## 3. Results and discussion

Figures 1(a)–(c) are STEM high angle annular dark field (HAADF) images projected along [010], [100], and [001] directions of the BIO film. All the atoms except for oxygen are shown as the white contrasted dots. The Ir atomic columns

have higher intensity contrast than the Ba atomic columns due to the larger atomic number  $Z$ . The projection images along [010] and [100] directions clearly show that the BIO crystal has a layered structure, with  $c \sim 25.535$  Å. The projection image along [100] shows that this layered structure consists of two distinguished ‘A’ and ‘B’ layers. ‘A’ layers are arrow-like, alternately pointing toward left or right, with each ‘arrow’ consisting of two Ir atoms in the middle and three Ba atoms with one at the arrow head and two at the arrow tail; ‘B’ layers are chain-like, with each segment consisting of an Ir atom and four Ba atoms. Based on the number of Ba and Ir atoms in the unit cell, which is deduced from three projections, and the fact that Ir ion has a valence of  $4+$  or  $5+$ , we derived the chemical formula for BIO to be  $\text{Ba}_7\text{Ir}_3\text{O}_{13+\delta}$ . Energy dispersive x-ray spectroscopy measurements on the BIO films have indeed shown that the Ba-to-Ir ratio is 70.1:29.9. From the projection images along three directions as well as the electron diffraction patterns along corresponding directions as shown in figures 1(e)–(g), an orthorhombic structure can be determined for the BIO film. From the diffraction patterns, the lattice constants for the BIO film are determined to be  $a = 5.960$  Å,  $b = 10.365$  Å, and  $c = 25.535$  Å. It is interesting to note that the STEM-HAADF image along [001] projection (figure 1(c)) shows a hexagonal arrangement of atoms. However, the high resolution TEM image (HRTEM) along the same direction (figure 1(d)), which contains the atomic structure information along the  $Z$  direction through dynamical scattering, reflects the true nature of an orthorhombic structure on  $ab$  plane.

The insulating properties of BIO films have been verified by optical spectroscopy measurements and transport measurements. We measured the real part of the optical conductivity of the BIO/STO film using variable-incidence-angle ellipsometry at room temperature. Figure 2 shows the real part of the optical conductivity for the BIO/STO (111) film at the room temperature. It can be seen clearly that the optical band gap of BIO is 1.3 eV at room temperature. The band gap is much higher than the gaps of any other known insulating iridate compounds ( $\sim 0.1$  eV for  $\text{Sr}_2\text{IrO}_4$  [13], and 0.34 eV for  $\text{Na}_2\text{IrO}_3$  [14]). We can get more insight into the origin of the optical conductivity features of BIO by further comparing its optical properties to the properties of the perovskite  $\text{Sr}_2\text{IrO}_4$ . The lowest energy ( $\sim 0.5$  eV) optical transitions of  $\text{Sr}_2\text{IrO}_4$  were interpreted as the transitions between upper and lower  $J_{\text{eff}} = 1/2$  Hubbard bands formed from the spin-orbit split  $t_{2g}$  levels, while the O  $2p$ -Ir  $5d$  charge-transfer transitions were found at energies over 3 eV [2, 13, 15]. The crystal-field splitting between  $t_{2g}$  and  $e_g$  states in the  $5d$  manifold was found to be 2.1 eV [15], and the  $t_{2g}$  states are further split by the relativistic spin-orbit coupling into  $J_{\text{eff}} = 1/2$  and  $J_{\text{eff}} = 3/2$  states [2]. We tentatively assign the two broad peaks A and B at 1.8 and 2.5 eV in figure 2 to the transitions from the spin-orbit split  $t_{2g}$  levels to the  $e_g$  levels of the nearest-neighbor Ir ions because their energy is so much higher than the splitting between the lower and upper Hubbard bands found in perovskite iridates (0.5/1.0 eV) [2, 13]. This assignment would imply that the spin-orbit splitting in BIO (0.7 eV) is higher than the splitting in the perovskite

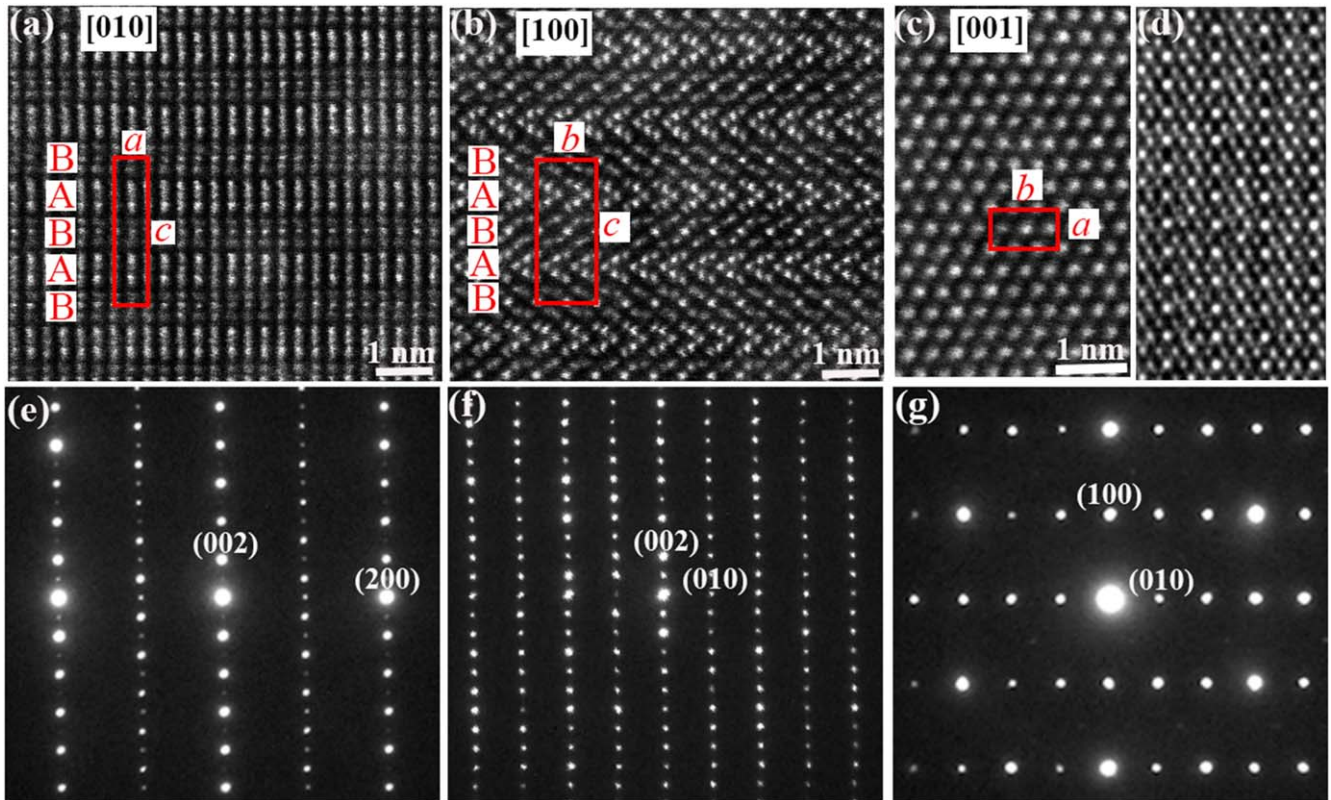


**Figure 1** STEM HAADF images for the BIO film projected along the (a) [010], (b) [100] and (c) [001] directions. (d) HRTEM image of the film along [001]. Electron diffraction patterns taken along (e) [010], (f) [100] and (g) [001] zone axis.

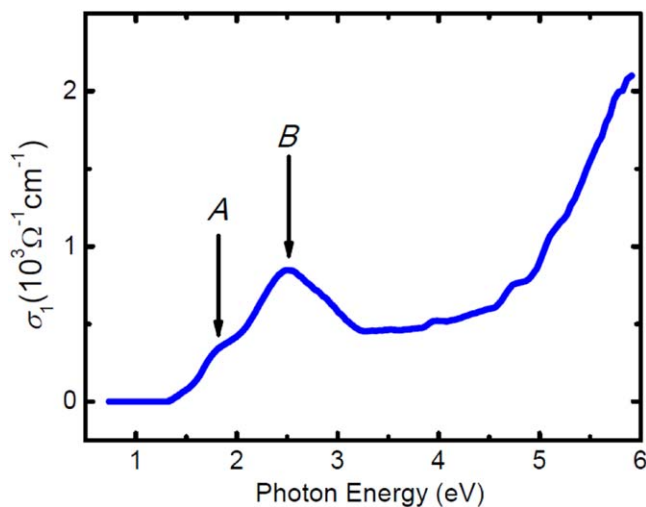


**Figure 2** The real part of the optical conductivity of the BIO/STO (111) film obtained from the ellipsometry measurements at room temperature.

$\text{Sr}_2\text{IrO}_4$  (0.4 eV), a finding that needs further confirmation by both experimental and theoretical means. The presence of the  $J_{\text{eff}} = 1/2$  Hubbard bands remains an open question in BIO, as the Ir–O octahedra share edges and not corners as in perovskite iridates [2, 13]. The room temperature in-plane resistivity of the BIO films is  $\sim 1.1 \times 10^5 \Omega \text{ cm}$ , five orders of magnitude larger than the in-plane resistivity of  $\text{Sr}_2\text{IrO}_4$ .

We have further investigated their crystal structures through HR-XRD measurements. The films on all three

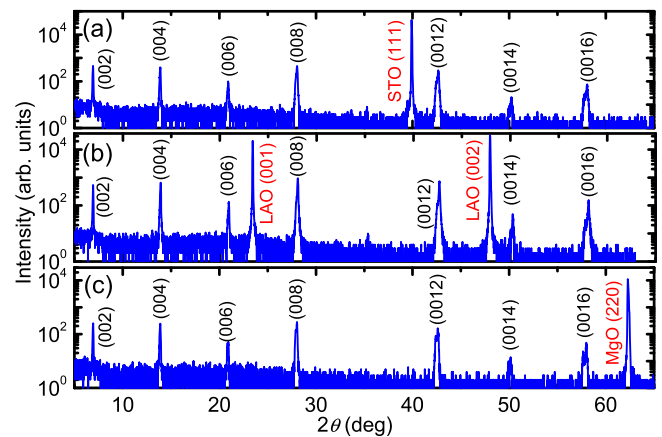


**Figure 3** HR-XRD  $\theta$ - $2\theta$  scans of 277 nm thick BIO films on (a) the STO(111) substrate, (b) the LAO(001) substrate and (c) the MgO (110) substrate.

substrates show crystallization with the  $c$ -orientation perpendicular to the substrate surfaces, regardless of the substrate orientation, which can be clearly seen from the strong (00 $l$ ) diffraction peaks in the  $2\theta$ - $\theta$  scans, as shown in figures 3(a)–(c). Such a substrate-orientation-independent  $c$ -oriented growth for BIO films strongly suggests the existence of multiple domains, as the crystalline symmetry of the BIO films and the substrates are incompatible. To confirm this, we performed HR-XRD  $\varphi$  scans for the (0 4 18) reflections of BIO/STO (111) and BIO/LAO (001) films and the (2 0 16) reflection of BIO/MgO (110) films, as shown in figures 4(a)–

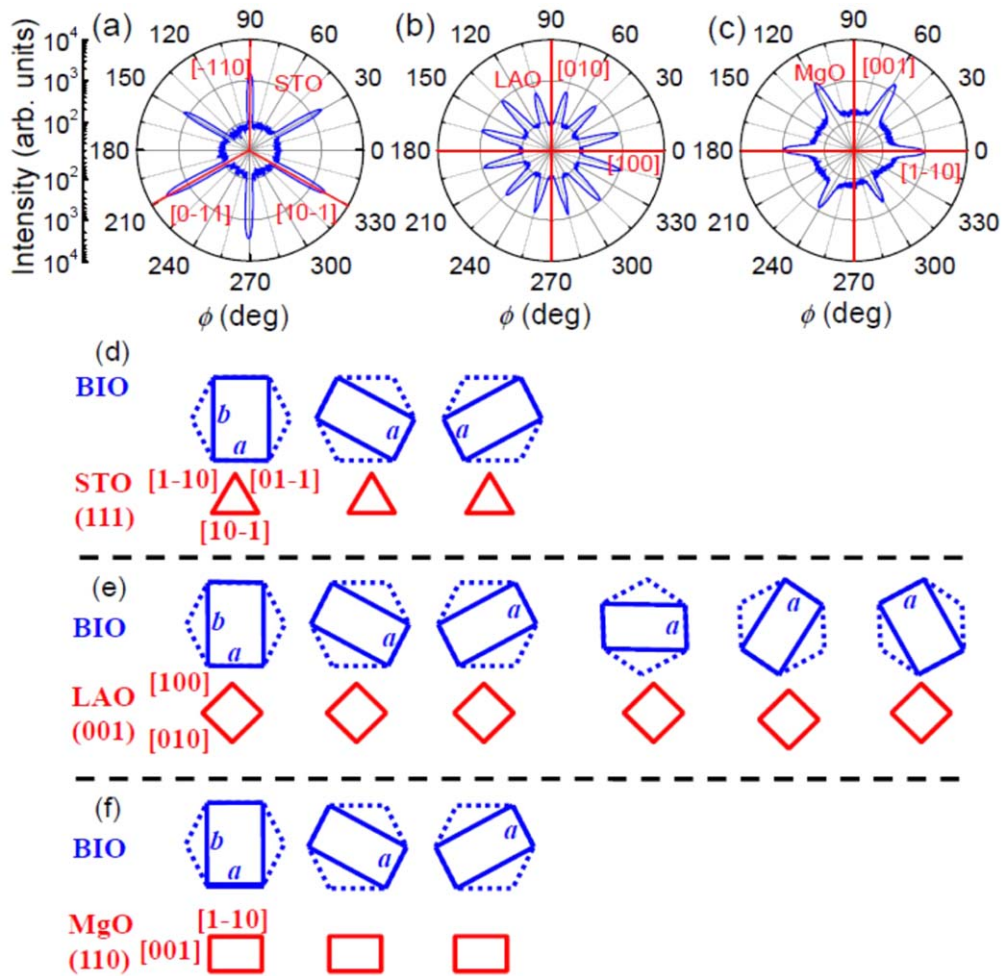


**Figure 4** HR-XRD  $\phi$  scans of the BIO (0 4 18) reflection for (a) the BIO/STO(111) film, (b) the BIO/LAO(001) film; (c)  $\phi$  scan for the BIO (2 0 16) reflection for the BIO/MgO(110) film. Schematic diagrams of epitaxial relationships for (d) the BIO/STO(111) films, (e) the BIO/LAO(001) films, and (f) the BIO/MgO(110) films. The solid lines represent the BIO and substrate lattices, and the dashed lines represent the hexagonal atomic arrangement on the  $ab$ -plane.

(c), respectively. The 12 fold diffraction peaks for BIO/LAO (001) (figure 4(b)) indicate the existence of six domain orientations, since each orthorhombic domain contributes two peaks in the  $\phi$  scan. For BIO/STO (111) (figure 4(a)) and BIO/MgO (110) (figure 4(c)) films, the 6 fold diffraction peaks indicate that there are three domain orientations. We also noticed that the BIO/STO (111) films have the sharpest  $\phi$  scan peaks, whereas the BIO/MgO (110) films have the widest peaks, suggesting the domain coherence is the best for the BIO/STO (111) films, but the worst for the BIO/MgO (110) films. Such a substrate dependent domain coherency is possibly due to the distinct symmetry mismatching between BIO films and substrates.

The distinct domain structures among these three types of films can be understood in terms of epitaxial relationships. Since the orthorhombic structure of BIO films is characterized by the hexagonal arrangement of atoms on the basal plane as shown in figure 1(c) and the lattice constant  $a$  of BIO films are close to  $\sqrt{2}$  times the lattice parameter of cubic oxide substrates, the  $[100]_{\text{BIO}}$  axis would favor to align with  $[110]$ -equivalent crystal axes of the substrates. From this

perspective, combined with the domain information revealed from the XRD  $\phi$  scans, we can speculate potential domain orientations on each substrate, as illustrated in figures 4(d)–(f). The relative orientation angle between the domains is expected to be  $60^\circ/120^\circ$  for the BIO/STO (111) and BIO/MgO (110) films (figures 4(d) and (f)), but either  $60^\circ/120^\circ$  or  $90^\circ$  for the BIO/LAO (001) film (figure 4(e)).

To observe the expected domains and domain walls, we performed TEM imaging on these BIO films. For the BIO/STO (111) film, as seen in the inset to figure 5(a), it shows an electron diffraction pattern with a 6 fold symmetry, indicating the existence of 3 domains, consistent with the result of the XRD  $\phi$  scan. Interestingly, the domain-walls as expected from figure 4(d) are not visible either for the  $[001]$  projection in low magnification bright field (BF) TEM image (figure 5(a)) nor in STEM HAADF imaging (figure 5(c)). However, they show up in HRTEM imaging due to the dynamical diffraction interferences from all directions, as shown in figure 5(b). Here the two domains are rotated by  $120^\circ$  relative to each other. These domain-walls are

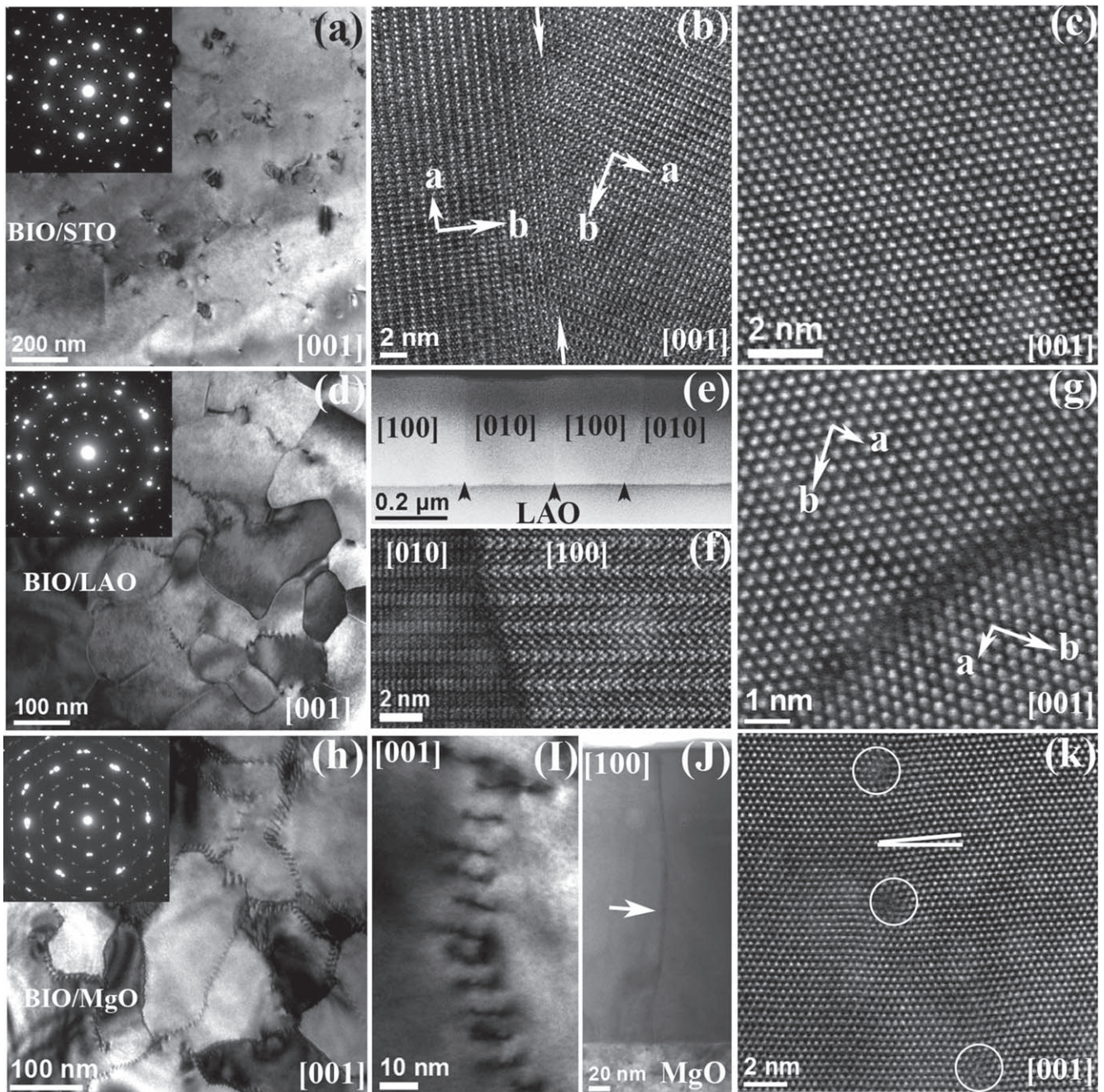


**Figure 5.** (a)–(c) TEM/HRTEM images of the BIO/STO(111) film projected along [001]; (a) low magnification BF TEM image and the inset showing the electron diffraction pattern along [001]; (b) HRTEM image of type I domain-wall; (c) STEM HAADF image showing no domain-wall. (d)–(g) TEM images of the BIO/LAO(001) film; (d) low magnification BF TEM image projected along [001] and the inset showing the electron diffraction pattern along [001]; (e) cross-sectional STEM HAADF side image of the film at low magnification showing 90° domains; (f) high magnification STEM HAADF image of the side view of the 90° domain-wall; (g) STEM HAADF image of the 90° domain-wall along [001]. (h)–(k) TEM images of the BIO/MgO(110) film; (h) low magnification BF TEM image and the inset showing electron diffraction pattern along [001]; (i) enlarged BF TEM image of the domain-wall showing dislocation array; (j) BF TEM image of the cross sectional view of the film showing the dislocation threading through the whole film; (k) STEM HAADF image of the film along [001] showing the end on domain-wall dislocations (circled).

*atomically thin* (denoted by type I domain-walls hereafter), coherently connecting atoms with hexagonal arrangement.

For BIO/LAO (001) film, in addition to type I domain-walls, the expected domain-wall characterized by a 90° rotation (see figure 4(e)) is indeed observed, as shown in figures 5(d)–(g). The electron diffraction pattern over the

whole area of figure 5(d) exhibits a 12 fold symmetry (inset to figure 5(d)), indicating the existence of 6 domain orientations, in agreement with the HR-XRD  $\varphi$  scan results. Figures 5(e) and (f) are HAADF-STEM cross sectional images of the BIO/LAO (001) film, which show the 90° domain-walls (type II). Type II domain-walls show up as continuous dark

lines in low magnification BF image (figure 5(d)). The 90° domain rotation can also be clearly seen from the atomic structures on the (001) plane as shown in figure 5(g). Like type I domain-walls, type II domain-walls are also atomically sharp, ~2–3 atoms thick. Apparently, type II domain-walls can be attributed to two hexagonal atomic arrangements on the basal plane oriented perpendicularly to each other, as shown in figure 4(e). They start to form from at the film/substrate interface and thread through the whole film to the film surface (figure 5(e)).

For the BIO/MgO (110) film, while it is expected to exhibit similar domain orientations as the BIO/STO film as shown in figure 4(f), it exhibits additional defects besides type I domain-walls. As seen in the inset to figure 5(h), although the BIO/MgO (110) film also exhibits an electron diffraction with a 6 fold symmetry along the [001] projection, the diffraction spots show a dispersion of ~7°, indicating that its domain orientation is more random as compared to BIO/STO (111) films. This is also exactly what we have seen in the HR-XRD  $\varphi$  scan where the peaks representing three different domain orientations look much broader than the other two types of films. From the low magnification BF TEM images (figures 5(h) and (I)), networks of line defects can be clearly seen and these line defects form a new type of domain boundaries (type III). The typical dislocation contrast of line defects arises from the electrons deflected strongly by the distorted atomic planes around the dislocation cores [16]. These individual dislocations thread through the whole film from the film/substrate interface to the film surface (figure 5(J)). The atomic structure of the projected dislocation cores is presented in figure 5(k), where these dislocations have a Burgers vector of [100] by drawing Burgers circuit around the core. Those two white lines indicate the atomic planes across the boundary have ~7° deviation in orientation, consistent with the ~7° dispersion seen in the electron diffraction. The presence of such line defect networks should be associated with the low symmetry of MgO (110) surface which limits the capability of substrates to pin the direction of BIO domains.

The above results clearly demonstrate that we can control the domain symmetries and domain wall qualities via the geometric design of the epitaxy. Such a unique property is not seen in other epitaxial systems where the crystalline orientations of the film follow those of the substrate. We believe that the ultra-long  $c$ -axis of the film ~25.535 Å implies a largely anisotropic surface energy of the film, leading to  $c$ -oriented growth regardless of the substrate orientation. Therefore, in terms of epitaxial relationship, the only degree of freedom is the rotation of the film lattice about  $c$ -axis. In order to match the surface lattice of the substrate, the lattice of BIO film rotates about  $c$ -axis accordingly, leading to different domain symmetries and domain-wall qualities for different substrate orientations. The above results provide a unique geometric method to engineer the domain symmetry and domain-walls. BIO films possess the widest band gap among all iridate compounds. This material reveals a unique playground to investigate strong SOC in iridates, whereas the domain walls

in BIO films provide a unique opportunity to search for exotic states derived from SOC-induced Mott states.

#### 4. Summary

We have discovered a new phase of iridate, Ba<sub>7</sub>Ir<sub>3</sub>O<sub>13+ $\delta$</sub>  (BIO), in thin film form. This material possesses a layered orthorhombic structure and is insulating, with a gap ~1.3 eV (which is the largest among all known iridates). The BIO films can be grown on differently oriented perovskite substrates or MgO substrates and they all show the same orientations, with the  $c$ -axis perpendicular to the substrate surfaces. Due to in-plane lattice mismatch, the BIO films show substrate-dependent domain walls. We observed highly coherent and atomically sharp domain walls on the films grown on the SrTiO<sub>3</sub> (111) and LaAlO<sub>3</sub> (001) substrates. The BIO films on the MgO (110) substrates, however, exhibit much less coherent domains and thread dislocations at the domain-walls. These results not only provide a new playground for investigating novel SOC physics in iridates, but also open a promising route to engineer domain symmetries and high quality domain-walls using geometric constrain from the substrates.

#### Acknowledgments

We acknowledge financial support by the US Department of Defense Army Research Office under grant No. W911NF0910530 and by the Florida State University Research Foundation, National High Magnetic Field Laboratory (NSF-DMR-0654118) and the State of Florida.

#### ORCID iDs

Ludi Miao  <https://orcid.org/0000-0002-4083-8735>

#### References

- [1] Cao G and Schlottmann P 2018 The challenge of spin-orbit-tuned ground states in iridates: a key issues review *Rep. Prog. Phys.* **81** 042502
- [2] Kim B J *et al* 2008 Novel  $J_{\text{eff}} = 1/2$  mott state induced by relativistic spin-orbit coupling in Sr<sub>2</sub>IrO<sub>4</sub> *Phys. Rev. Lett.* **101** 076402
- [3] Moon S J, Jin H, Choi W S, Lee J S, Seo S S A, Yu J, Cao G, Noh T W and Lee Y S 2009 Temperature dependence of the electronic structure of the  $J_{\text{eff}} = 1/2$  Mott insulator Sr<sub>2</sub>IrO<sub>4</sub> studied by optical spectroscopy *Phys. Rev. B* **80** 195110
- [4] Kim B J, Ohsumi H, Komesu T, Sakai S, Morita T, Takagi H and Arima T 2009 Phase-sensitive observation of a spin-orbital mott state in Sr<sub>2</sub>IrO<sub>4</sub> *Science* **323** 1329
- [5] Yang B-J and Kim Y B 2010 Topological insulators and metal-insulator transition in the pyrochlore iridates *Phys. Rev. B* **82** 085111
- [6] Kim C H, Kim H S, Jeong H, Jin H and Yu J 2012 Topological quantum phase transition in 5d transition metal oxide Na<sub>2</sub>IrO<sub>3</sub> *Phys. Rev. Lett.* **108** 106401

- [7] Carter J-M, Shankar V V, Zeb M A and Kee H-Y 2012 Semimetal and topological insulator in perovskite iridates *Phys. Rev. B* **85** 115105
- [8] Shitade A, Katsura H, Kuneš J, Qi X-L, Zhang S-C and Nagaosa N 2009 Quantum spin hall effect in a transition metal oxide  $\text{Na}_2\text{IrO}_3$  *Phys. Rev. Lett.* **102** 256403
- [9] Wan X, Turner A M, Vishwanath A and Savrasov S Y 2011 Topological semimetal and fermi-arc surface states in the electronic structure of pyrochlore iridates *Phys. Rev. B* **83** 205101
- [10] Chaloupka J, Jackeli G and Khaliulin G 2010 Kitaev–Heisenberg model on a honeycomb lattice: possible exotic phases in iridium oxides  $\text{A}_2\text{IrO}_3$  *Phys. Rev. Lett.* **105** 027204
- [11] Wang F and Senthil T 2011 Twisted hubbard model for  $\text{Sr}_2\text{IrO}_4$ : magnetism and possible high temperature superconductivity *Phys. Rev. Lett.* **106** 136402
- [12] Takayama T, Kato A, Dinnebier R, Nuss J, Kono H, Veiga L S I, Fabbri G, Haskel D and Takagi H 2015 Hyperhoneycomb iridate  $\beta\text{-Li}_2\text{IrO}_3$  as a platform for kitaev *Magn. Phys. Rev. Lett.* **114** 077202
- [13] Moon S J *et al* 2008 Dimensionality-controlled insulator-metal transition and correlated metallic state in 5d transition metal oxides  $\text{Sr}_{n+1}\text{Ir}_n\text{O}_{3n+1}$  ( $n = 1, 2, \text{ and } \infty$ ) *Phys. Rev. Lett.* **101** 226402
- [14] Comin R *et al* 2012  $\text{Na}_2\text{IrO}_3$  as a novel relativistic mott insulator with a 340-meV gap *Phys. Rev. Lett.* **109** 266406
- [15] Moon S J *et al* 2006 Electronic structures of layered perovskite  $\text{Sr}_2\text{MO}_4$  ( $M = \text{Ru, Rh, and Ir}$ ) *Phys. Rev. B* **74** 113104
- [16] Hirsch P B, Horne R W and Whelan M J 1956 Direct observations of the arrangement and motion of dislocations in aluminium *Phil. Mag.* **1** 677